Site-specific hydrogen-atom elimination in photoexcited ethyl radical

David V. Chicharro,[a‡] Sonia Marggi Poullain,[b‡],Alexandre Zanchet,[a,c] Aymen Bouallagui,[c,d] Alberto García-Vela,[c] María L. Senent,[e] Luis Rubio-Lago[a] and Luis Bañares[a]

Supporting Information

[0a] *Departamento de Química Física (Unidad Asociada I+D+i al CSIC), Facultad de Ciencias Químicas, Universidad Complutense de Madrid, 28040 Madrid, Spain. Tel: +34 913944228; E-mail: lbanares@ucm.es*
[0b] *Departamento de Química, Módulo 13, Facultad de Ciencias, Universidad Autónoma de Madrid, 28049 Madrid, Spain.*
[0c] *Instituto de Física Fundamental, Consejo Superior de Investigaciones Científicas, C/ Serrano, 123, 28006 Madrid, Spain.*
[0d] *Laboratoire de Spectroscopie Atomique, Moléculaire et Applications-LSAMA LR01ES09, Faculté des Sciences de Tunis, Université de Tunis El Manar, 2092, Tunis, Tunisia.*
[0e] *Departamento de Química y Física Teóricas, Instituto de Estructura de la Materia, Consejo Superior de Investigaciones Científicas, C/ Serrano, 121, 28006 Madrid, Spain.*
[0‡] These authors contributed equally to this work

1 H-atom action spectra

H-atom fragment action spectra from the photodissociation of the CH_3CH_2I, CH_3CD_2I and CD_3CH_2I precursors and D-atom action spectrum from the photodissociation of the CD_3CD_2I precursor, as a function of the excitation wavelength, which varies in the 199.5-201.4 nm range, are depicted in Figure S1. We remark that the same nanosecond pump laser photodissociates the precursor molecule and excites the corresponding ethyl radical, while the H-atom (D-atom) fragment produced is detected in this case by a (2+1) resonance enhanced multiphoton ionization (REMPI) scheme at 243.1 nm (243.06 nm). See the main text for details about the experimental methodology employed.

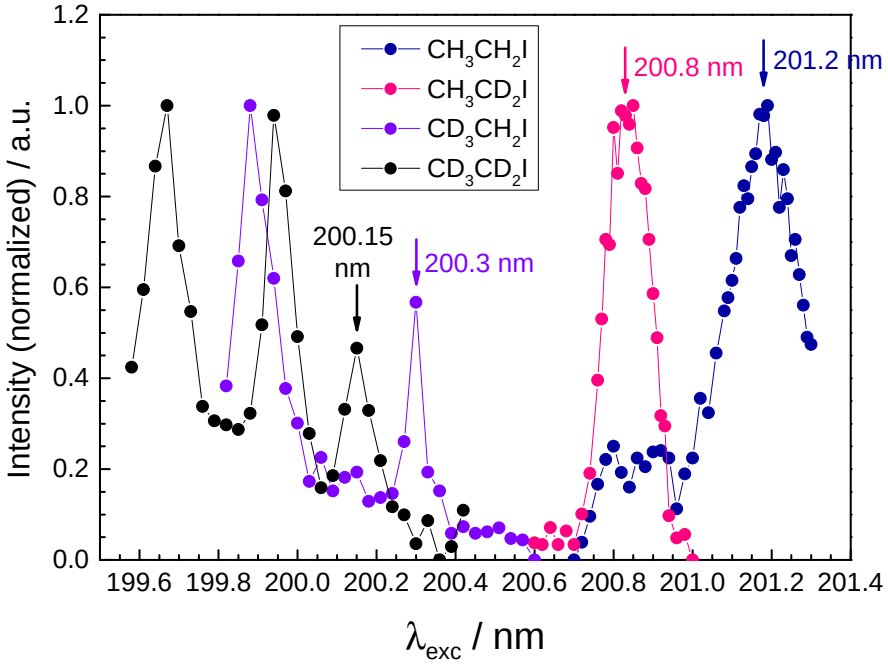

Figure S1: H-atom action spectra from the photodissociation of the CH_3CH_2I, CH_3CD_2I and CD_3CH_2I precursors as a function of the excitation wavelength, λ_{exc}. A (2+1) REMPI scheme at 243.1 nm is employed to detect the H-atoms produced from the secondary dissociation of the corresponding ethyl radical. Vertical arrows highlight the selected excitation wavelength corresponding to the origin 0_0^0 band for each isotopologue occuring at 201.2 nm for CH_3CH_2I, 200.8 nm for CH_3CD_2I and 200.3 nm for CD_3CH_2I. The D-atom action spectrum from the photodissociation of the CD_3CD_2I with D-atom detection at 243.06 nm is also depicted. The 0_0^0 band for CD_3CD_2I occurs at 200.15 nm.

2 D-atom images and translational energy distributions

The D-atom images measured are depicted in Fig. S2 along with the corresponding translational energy distribution. A weak ring is indeed observed in the image while a shoulder is recovered in the TED for the isotopologues CD_3CD_2 and CH_3CD_2.

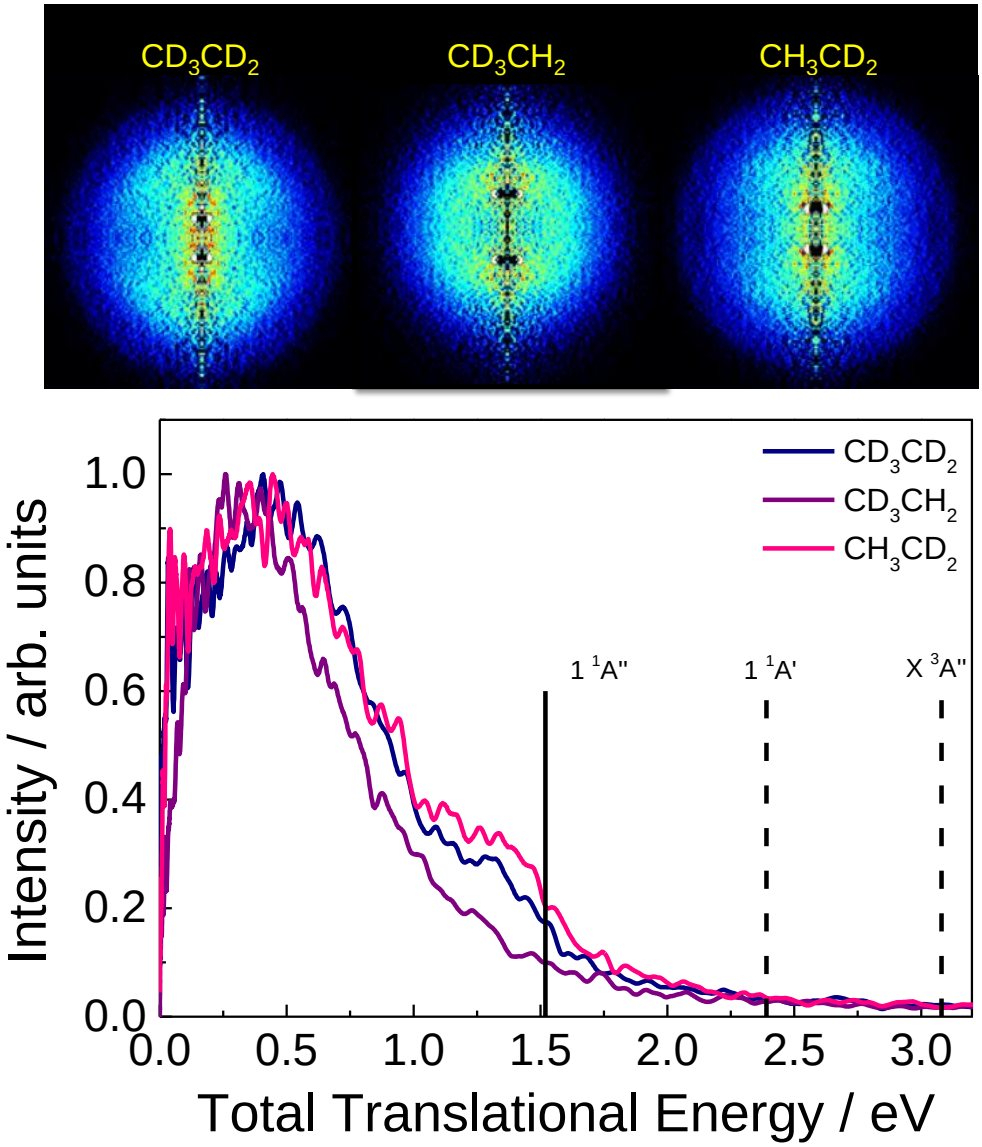

Figure S2: Top: D-atom Abel-inverted velocity map images for the three isotopologues CD_3CD_2, CH_3CD_2 and CD_3CH_2, excited at 200.15 , 200.8 and 200.3 nm, respectively (see Fig.S1). Bottom: Total translational energy distributions (TED) extracted from the images. Vertical bars specify the available energy for the three first C_α dissociation limits (see the text for more details). The TEDs have been normalized independently with respect to their corresponding intensity maximum.

3 Computed vibrational frequencies, zero-point energies and dissociation energies

The computed vibrational harmonic and anharmonic corrected frequencies for CH_3CH_2, CH_2CH_2 and CH_3CH are summarized in Tables 1, 2 and 3, respectively. We note that the model employed to estimate anharmonic correction is not adapted for non-rigid doublet species. See the main text for details about the computational methodology employed. Table 4 shows the harmonic and anharmonic corrected zero point energies for those species. In Table 5, the harmonic zero point energies along with the dissociation energies D_0 of all the isotopologues are summarized.

Table 1: Harmonic and anharmonic corrected vibrational frequencies of ethyl CH_3CH_2 radical in cm^{-1}.

Vibrational mode	Harmonic frequency	Anharmonic frequency
ν_1	3319.96	3186.11
ν_2	3210.54	3098.66
ν_3	3161.74	3009.03
ν_4	3115.07	2980.35
ν_5	3031.05	2942.54
ν_6	1509.02	1465.53
ν_7	1508.56	1460.03
ν_8	1493.82	1456.08
ν_9	1415.69	1377.71
ν_{10}	1211.56	1177.93
ν_{11}	1087.64	1064.21
ν_{12}	995.42	935.05
ν_{13}	817.53	821.46
ν_{14}	471.15	477.30
ν_{15}	134.40	-4.79*

Table 2: Harmonic and anharmonic corrected vibrational frequencies of the CH_3CH radical in cm^{-1}.

Vibrational mode	Harmonic frequency	Anharmonic frequency
ν_1	3277.52	3159.86
ν_2	3143.65	2996.24
ν_3	3099.27	2958.97
ν_4	3033.50	2928.73
ν_5	1490.14	1439.97
ν_6	1486.16	1441.37
ν_7	1407.18	1368.88
ν_8	1132.58	1081.39
ν_9	1101.70	1043.48
ν_{10}	1009.70	1007.46
ν_{11}	790.67	776.88
ν_{12}	194.41	125.07

Table 3: Harmonic and anharmonic corrected vibrational frequencies of ethylene CH_2CH_2 in cm^{-1}.

Vibrational mode	Harmonic frequency	Anharmonic frequency
ν_1	3288.60	3149.67
ν_2	3260.94	3126.90
ν_3	3191.86	3054.51
ν_4	3172.84	3011.40
ν_5	1677.76	1628.39
ν_6	1478.99	1445.19
ν_7	1379.59	1352.42
ν_8	1244.88	1231.31
ν_9	1047.13	1142.59
ν_{10}	945.70	1005.77
ν_{11}	975.49	967.71
ν_{12}	823.29	826.67

Table 4: Harmonic and anharmonic corrected vibrational zero-point energies (ZPE) of the corresponding species in cm^{-1}.

Species	Harmonic ZPE	Anharmonic ZPE
CH_3CH_2	13241.58	13025.94
CH_3CH	10583.24	10408.38
CH_2CH_2	11243.54	11155.92

Table 5: Harmonic zero-point energies (ZPE) and dissociation energies, D_0, of all the isotopologues in cm^{-1} and eV, respectively.

Species	Harmonic ZPE	D_0
CH_3CH_2	13241.58	4.35
CH_3CH	10583.24	–
CH_2CH_2	11243.54	–
CD_3CD_2	9799.4	4.45
CD_3CD	7752.69	–
CD_2CD_2	8495.65	–
CD_3CH_2	11003.72	4.36
CD_3CH	8290.85	–
CD_2CH_2	9878.8	–
CH_3CD_2	11893.74	4.44
CH_3CD	9787.22	–

4 Conical Intersections

The resulting geometries from the optimization of the three conical intersections found are shown in Fig. S3.

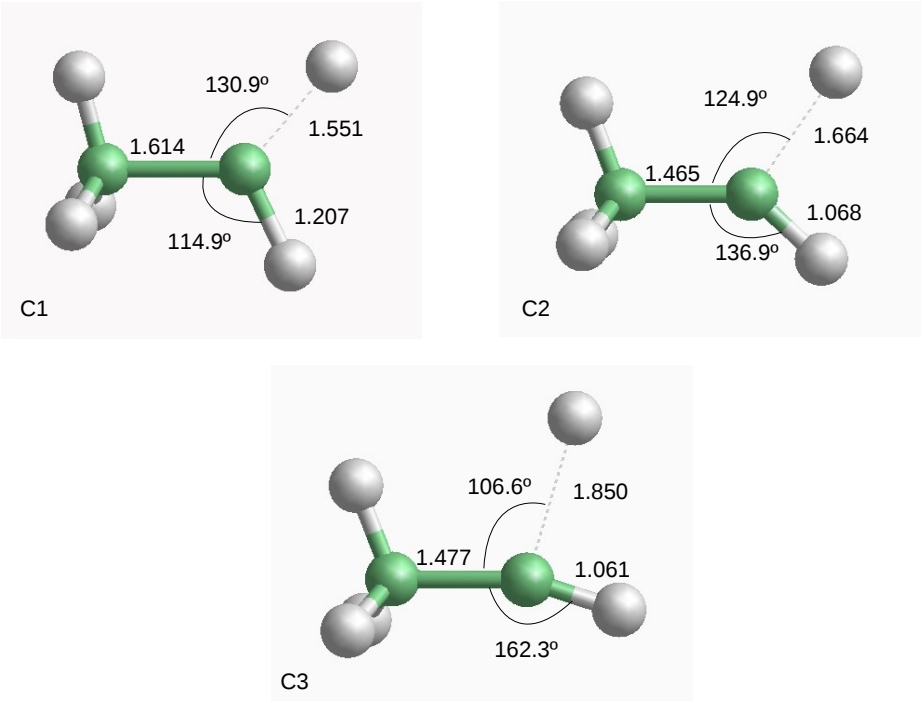

Figure S3: Geometries of the three conical intersections found and optimized, labelled C1, C2 and C3.